Flexibility of C-S-H sheets and stacks from molecular simulations

Tulio Honorio, Laurent Brochard

2nd International RILEM/COST Conference on Early Age Cracking and
Serviceability in Cement-based Materials and Structures - EAC2
12–14 September 2017, ULB-VUB, Brussels, Belgium

Flexibility of C-S-H sheets and stacks from molecular simulations

Tulio Honorio *[a], Laurent Brochard[a]
[a]Université Paris-Est, Laboratoire Navier (UMR 8205), CNRS, ENPC, IFSTTAR, 6 & 8 Avenue Blaise Pascal, 77455 Marne-la-Vallée, France

ABSTRACT

The flexibility of C-S-H solid sheets may play, as is the case of other phyllosilicates, an important role in the structuration of "bulk" C-S-H. In this paper, we determine, for the first time to the author's knowledge, the bending modulus of tobermorite single sheets by the combination of molecular simulations and Kichhoff-Love plate theory. Further, using the results for laminates, we compute the bending modulus of stacks of solid layers, which are a larger structural unit in the nanotexture of phyllosilicates. Tobermorite single layers are more rigid than other phyllosilicates such as montmorillonites and kaolinites. Our estimation of shear stresses within a stack of layers, confronted to the yield strength of tobermorite computed by other authors, indicates that these stacks might exfoliate if the number of solid layers exceeds few tens. Stacks of this thickness are quite rigid, which justifies the choice of rigid grains in mesocale investigations of calcium silicate hydrates.

Keywords: Calcium silicate hydrates, Molecular simulation, Bending modulus, Nanotexture.

1. INTRODUCTION

Phyllosilicates are a class of silicates structured in layers at the molecular scale. Clays and calcium silicate hydrates – including both the crystalline minerals such as tobermorite or disordered C-S-H – are examples of these layered silicates. Generally, in larger scales, other structural units are defined in order to understand the behavior of such materials. For example, smectite clays layers often present stacked structures with few solid layers. Similarly, C-S-H is reported to locally display an ordered (or stacked) structure. Mesoscale investigations of calcium silicates often refer to these ordered domains as grains or particles. In such studies, a grain is represented as an individual rigid isotropic entity [1]. In the case of clays, the flexibility of single layers or thin particles is reported to be one aspect leading to the macroscopic cohesion of the material. This cohesion occurs since a layer may be a part of a stack in a given zone and, due to its flexibility, be a part of another stack (i.e. a domain with another orientation and translational arrangement) in other zone. The bending modulus of smectite layers has the order of magnitude of 10^{-17} N.m [2], which corroborates the argument of mixed entangled and stacked (Figure 1) nanotexture of some clays.

To date, to the knowledge of the authors, the flexibility of single calcium silicate hydrates sheets have not yet been computed. This information is fundamental to validate the hypothesis of rigid C-S-H grain as well as to better understand the microtexture of C-S-H. In this paper, following a strategy developed in a previous study applied to clays [2], we compute the bending modulus of tobermorite by a combination of molecular simulations and thin plate and laminates theory. We discuss the implications of the bending modulus in the configurations of calcium silicate single sheets and stacks. These results go towards a better understanding of C-S-H structuration at sheet and grain scales.

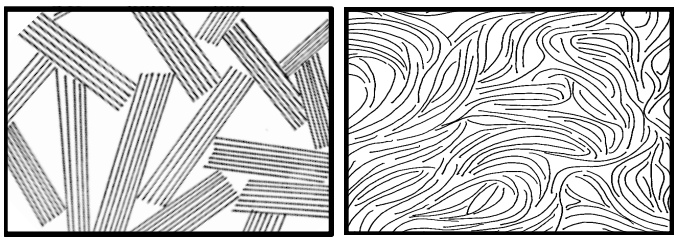

Figure 1. Extreme microtexture types of phyllosilicates: (left) brick-like or stacked (right) sheet-like or entangled (adapted from Honorio et al.[2])

*tulio.honorio-de-faria@enpc.fr; phone (+33) 1 64 15 36 59

2. MOLECULAR SIMULATION OF CALCIUM SILICATES

We simulate Hamid's [3] structure of tobermorite 11 Å with molar Ca/Si ratio of 1: $Ca_6[Si_6O_{18}]$. $2H_2O$. The average Ca/Si ratio of C-S-H phases present in commercial cements ranges from 2.3 to 0.7, with compositional heterogeneities at a scale of roughly 100 nm [4]. A molar Ca/Si ratio close to 1 is particularly relevant to applications in oil well cementing [5]. Figure 2 shows the monoclinic (a = 6.69 Å, b = 7.39 Å, c = 22.77 Å and $\gamma = 123.49°$) and pseudo orthorhombic cells, as proposed by Hamid [3]. The latter cell, defined here according to directions A' and B', is taken as reference in the computation of the elastic and bending modulus.

Among the different classical force fields applicable to C-S-H proposed in the literature, we choose CSHFF [6], which is based only in (pseudo-ionic) non-bonded Lennard-Jones interactions for metal and metalloids while harmonic bonds are only defined for water molecules and hydroxyls. We use the Lennard-Jones parameters, partial charges, angle and bond harmonic parameters of CSHFF as presented in the supporting information of Qomi et al. [7]. CSHFF have been extensively used in the computation mechanical properties of crystalline and disordered calcium silicates [8], which indicates its transferability to the estimation of the flexibility of tobermorite layers. Calcium counterions are added to the interlayer space in order to ensure the electroneutrality of the system. The partial charge of bridging oxygens are adjusted, in the limits of modified CSHFF [7], to exactly compensate the charges of calcium counterions. At the end, the surface change density of the tobermorite layer is -0.55 $C.m^{-2}$, which is close to the experimental value of -0.5 $C.m^{-2}$ [9].

The reference monoclinic cell of tobermorite is replicated 12 times in the direction of a or b unit vector, in order to generate a thin layer so that thin plate theory can be applied. Figure 2 displays the resulting thin layer for both in-plane directions in an orthographic view with respect to A' and B' directions. The aspect ratio of the simulated layers are $L_c/L_a = 0.0702$ (direction A') and $L_c/L_b = 0.0636$ (direction B'). The simulations are performed with LAMMPS [10] in the canonical ensemble (NVT) at 0.1 K with Nosé-Hoover thermostat. Since only the solid layer is considered, the temperature is deemed to not significantly affect the elastic properties. Moreover, with a temperature close to 0 K, the configurations energetically near the ones minimizing the potential energy of the system are sampled. A cutoff distance of 10 Å is adopted for short-range dispersive interactions and Ewald's summation method with accuracy of 10^{-5} for forces is employed with long-range electrostatic interactions. Simulations were run with periodic boundary conditions. To reduce the influence of periodic images on the behavior in c direction, 4 nm were added to the length of the simulation box in that direction.

A simulation point (for a given in-plane direction) is obtained by applying a displacement $\delta_i = \delta_{i-1} + \Delta\delta$, with $\Delta\delta = 0.1$ Å, imposed at the distance of one-quarter from each edge of the simulation box, as shown in Figure 2. For each displacement the system was equilibrated during 20 ps and sampled during 10 ps. The final configuration with displacement δ_i was used as the initial configuration for δ_{i+1}. The elastic free energy of bending W_i was determined from the difference between the potential energy at relaxed state U_0 and potential energy U_i associated to δ_i. Five different configurations were tested, in order to account for the influence of the position of counterions. For each configuration, Ca ions were randomly located in the interlayer space of original supercell before replication. The standard deviation in the free elastic energy of bending is provided with respect to these 5 simulations. The interlayer water and its likely screening effect is neglected, as previously done before in investigations of clay layers flexibility [11].

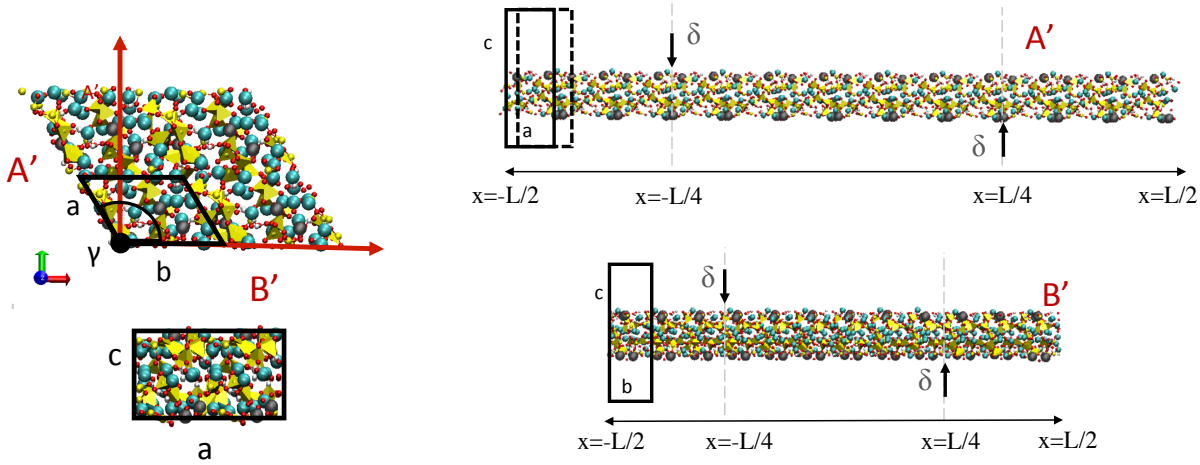

Figure 2. Snapshot of the structure of Hamid's [3] 11 Å tobermorite with Ca/Si = 1. The vectors a, b and c of the monoclinic cell and the directions A' and B' of the pseudo orthorhombic cell (considered hereafter in the simulations) are shown. Ca counterions are depicted as gray spheres; O atoms are red sticks, H white sticks, Si yellow tetrahedron, Ca (within the solid) green spheres.

3. RESULTS

Bending modulus of a single layer

The bending modulus of a thin plate can be computed by means of the test in Figure 2 (right) with the formula [2]:

$$D_a = \frac{W}{6}\left(\frac{L}{4}\right)^3 \frac{1}{\delta^2} \quad (1)$$

where L is the length of the layer in a direction and δ is the imposed displacement in the flexion test of Figure 2. We assume 1) smooth bending (the position of neighboring atoms remains correlated through bending), 2) orthogonal section remaining straight and orthogonal to the mid-plane, 3) constant thickness of the layer and 4) infinitesimal deformation. Figure 3 shows the elastic free energy of bending obtained by molecular simulation. Similar smooth curves fitting a quadratic law are found for clays [2]. Possible structural changes induced by the displacement δ are not observed to the displacements δ up to 2 Å. In this case, the bending modulus would be displacement dependent. With these results and Eq. (1), we estimate bending moduli reflecting the average flexural behavior for displacements up to 2 Å. The obtained bending moduli (Table 1) are one order of magnitude larger than the bending modulus estimated for other phyllosilicates such as montmorillonite (1.87-2.02 x 10^{-17} N.m) or kaolinite (0.51-0.73 x 10^{-17} N.m)[2].

The in-plane Young modulus in a direction a can be computed from the bending modulus and the effective "mechanical" thickness h of the layer by [12]:

$$E_a = D_a \frac{12(1-\nu^2)}{h^3} \quad (2)$$

Table 1 gathers the estimations of Young modulus. Two effective thickness are considered: (1) h_s=12.0 Å, corresponding to the distance between the center of outmost atoms in each external surface after relaxation; and (2) h_s=15.44 Å, corresponding to the previous distance plus twice the van der Waals radius of oxygen. The estimations with h_s=15.44 Å are closer to the values of Young moduli obtained by other techniques. For the sake of comparison, we also determined the in-plane coefficients of stiffness tensor through fluctuation formula of Parrinello-Rahman [13]:

$$C_{ijkl} = \frac{k_b T}{\langle V \rangle_{NPT}} \left[\langle \varepsilon_{ij} \varepsilon_{kl} \rangle_{NPT} - \langle \varepsilon_{ij} \rangle_{NPT} \langle \varepsilon_{ij} \rangle_{NPT} \right]^{-1} \quad (3)$$

where k_b is the Boltzmann constant, T is the temperature, V is the volume, $\langle . \rangle_{NPT}$ is the average operator in the isothermal-isobaric (NPT) ensemble, and ε_{ij} is the strain tensor. For a triclinic simulation box, $\varepsilon_{ij} = \frac{1}{2}\left[\left(h_{0,ik}^{-1}\right)^t h_{kl}^t h_{lm} h_{0,m}^{-1} - \delta_{ij} \right]$, with $h_{0,ik}$ and h_{ik}being the components of cell matrices in the reference and deformed states, respectively; and δ_{ij} is the delta of Kronecker. The Young modulus can be computed from the in-plane components of stiffness tensor by $C_{iiii} = E_i/(1-\nu^2)$, assuming that the in-plane Poisson ratio of calcium silicate hydrates $\nu_{ab} = \nu_{ba} = \nu = 0.3$ [6]. Shahsavari et al. [6] computed, by first principles methods, the full stiffness tensor of Hamid's tobermorite with Ca/Si = 1 and obtained (after rotation to our reference frame) 122.36 and 19.26 GPa in A' and B' direction, respectively. The in-plane elastic moduli of tobermorite are similar to the ones of other phyllosilicates (e.g. circa 250 GPa for montmorillonite or 150-200 GPa for kaolinite [2]). The estimations of the elastic modulus of tobermorite, obtained from different techniques, are in reasonable agreement for the purposes of this study. Note that the bending modulus scales linearly with E_a, and bending moduli with the same order of magnitude might lead to similar implications. On the other hand, the bending modulus scales with h^3 (Eq. 2). The larger thickness of tobermorite solid layers explains most of the higher bending modulus when compared to other phyllosilicates (for example, h_s is circa 9.15 Å for montmorillonite and 7.3 Å for kaolinite [2,14]).

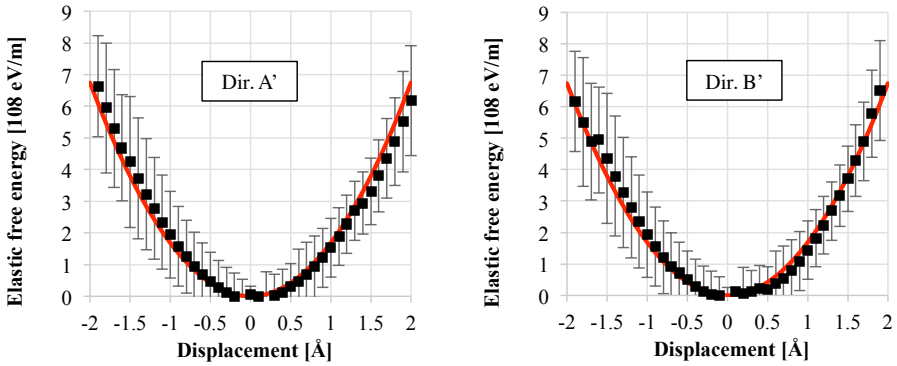

Figure 3. Elastic free energy for flexion test in A' and B' directions. The red curve is the fitted harmonic potential.

Table 1. Bending and Young moduli in A' and B' directions.

Direction	Bending modulus (10^{-17} N.m)	Young modulus (GPa) from fluctuation formula (Eq. 3) with NPT simulation	Young modulus (GPa) with Eq. 2	
			h_s=12.00 Å	h_s=15.44 Å
A'	4.68 ± 1.74	269.0 ± 67.8	295.5	138.7
B'	1.42 ± 0.91	54.8 ± 13.8	89.5	42.03

Bending modulus of a stack of layers

The bending modulus of a stack of layers can be estimated by assuming a laminate of solid layers intercalated with a fluid phase. The behavior of confined fluids in nanopores differs from the behavior of bulk fluids: in some cases, solid-like and glassy behaviors are reported [15,16]. This aspect can be taken into account by associating an elastic shear bearing behavior to the confined fluid. The overall bending modulus of the stack, reads [2]:

$$D^p{}_a = \int_{-h/2}^{h/2} z^2 \, C_{aaaa}(z) dz \tag{4}$$

Let the total thickness of the stack be defined by $h = N.h_s + (N-1)(< e > - h_s)$, with N being the number of solid layers and $< e >$ being the average basal spacing. It can be shown [2] that $D^p{}_a$ scales with N^3. The basal spacing associated to the most pronounced energy well in face-to-face configurations is 22.8 Å for C-S-H according to Bonnaud et al. [17]. Figure 4 shows the bending modulus of a stack according to the number of solid layers with $< e >$ = 22.8 Å.

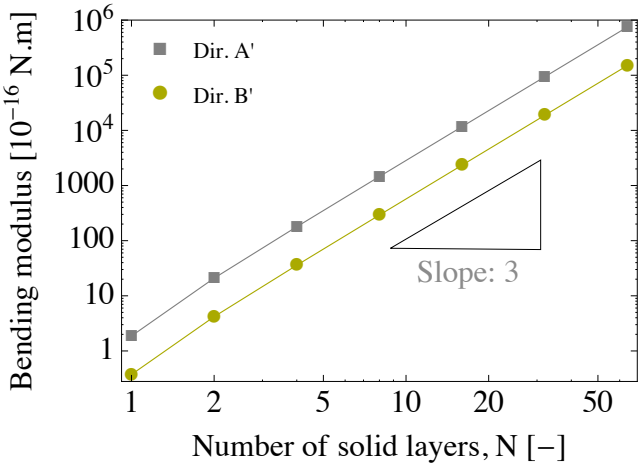

Figure 4. Bending modulus of a stack as a function of the number of solid layers for each in-plane direction A' and B'.

An estimation of the shear stresses along the thickness of the laminate can be computed by [2]:

$$\tau_{xz}(z) = -\frac{1}{(1-\nu^2)} \frac{\partial}{\partial x} (\nabla^2 . u_z) \int_z^{h/2} z \, E(z) dz \tag{5}$$

where u_z is the out-of-plane displacement according to a given load. Figure 5 (left) displays the average τ_{xz} over half laminate (from x=0 to L/2), for a loading distributed load f as depicted in Figure 5 (right). With this loading, the shear stresses reach a maximum (in absolute values) at x = ±L/4 and z = 0. The average shear stresses can be compared to the yield strength, associated to shear deformation of tobermorite layers. The yield strength of tobermorite and disordered C-S-H, obtained by molecular simulations [18], are 5.8 and 16.1 GPa, respectively. These values are three orders of magnitude larger than the ones reported for montmorillonite layers [19], which is a reflect of the strong cohesion of calcium silicate layers. The yield strength represents the maximum shear stresses that can be supported by the inter-layer fluid in a stack of layers without exfoliation. Our estimation indicates that even very long tobermorite particles (L > 500 nm) and with more than roughly 10 solid layers might not exfoliate under vigorous stirring (f in the order of 1 to 100 KPa). It is necessary to reach a load f in the order of the MPa in order to observe "mechanical" exfoliation of stacks with L = 500 nm; and f in the order of a few tens of MPa, for stacks with with L = 50 nm.

Compared to other phyllosilicates, such as smectites, tobermorite single layers are more rigid and tobermorite stacks exceeding few tens of solid layers are less prone to exfoliation. Thus, the resulting texture is more susceptible to present larger coherence lengths (i.e. a more "brick-like" structuration as in Figure 1 left) than clays'. Stacked textures present

larger porosity and open texture [20]; being, therefore, more permeable. Taking $u_z = L$ as the limit of high deformability of a sheet, it can be shown that the critical load (homogeneous with a pressure) to induce a large deformation has the order of magnitude of $f_{flex} = D^p{}_a/L^3 \approx D_a N^3/L^3$. With few tens of layers, the critical load is in the order of 100 MPa for L = 100 nm and approximates of the GPa with L tending to few tens of nanometers.

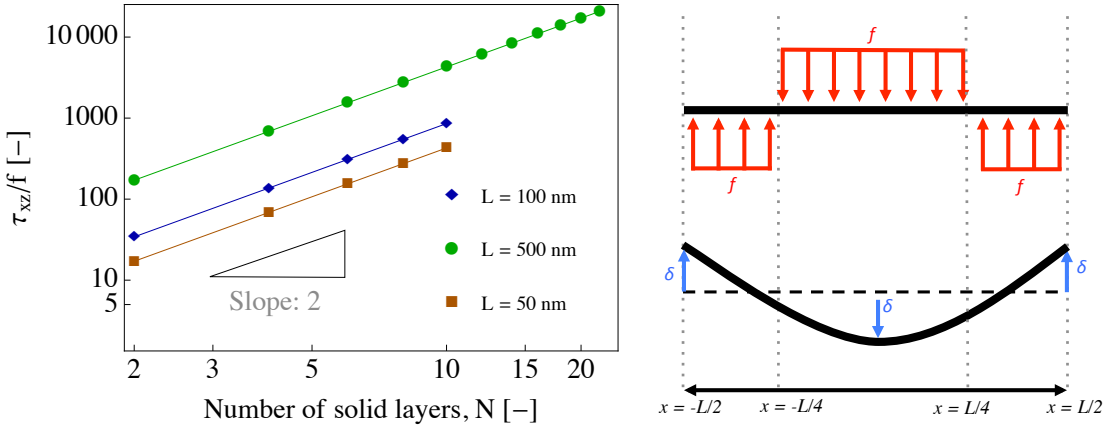

Figure 5. Average shear stresses in a half-length (from x=0 to L/2) of the laminate, as a function of the number of layers, for the loading depicted at the right with f = 1 kPa, represent a moderate solution stirring.

Colloidal simulations of C-S-H mesostructure, in general, assume isotropic grains with a particle size distribution ranging from only a few nanometers [1] up to a few tens of nanometers [21]. With these dimensions, the particles are indeed behaving in a rigid way. The nanostructure of calcium silicates is, though, anisotropic locally. Sheet-like (2D) and fibril-like (1D) morphologies are often associated to calcium silicates [4]. The in-plane dimensions of C-S-H (2D) sheets ranges in general from 30 to 60 nm [22]. So, with single sheets, a slight bent configuration may appears. Aged or heat-cured samples are reported to present fibrils being several micrometers long and more than 100 nm thick (i.e. roughly N = 100) [23]. The 1D character of the fibrils, however, favors bending in the thinner dimension. Moreover, bending may be responsible to some of the orientational order (not necessarily associated to translational order) observed in some samples over lengths of circa 100 nm [23]. The flexibility of calcium silicates can be, therefore, a fundamental aspect in the nanotexture of these materials.

4. CONCLUSIONS

In this paper, we provided, for the first time to the author's knowledge, the in-plane bending modulus of tobermorite, which may serve as a first indication of the flexural behavior of calcium silicates in general. We employed Hamid 11 Å structure with molar Ca/Si = 1. The obtained bending moduli are larger than the bending moduli of other phyllosilicates, notably due to the larger effective thickness of tobermorite single layers. Further, we provided estimations of the bending moduli of stacks of layers, which is one of the structural units defining the nanotexture of many phyllosilicates. The computation of the shear stresses within the stack reveals that exfoliation might occur only for stresses in the order of a MPa with long stacks. These results indicate that the resulting texture is prone to present larger coherence lengths when compared to clays. The order of magnitude of the bending modulus, however, does not exclude the existence of bent configurations of long single sheets or long stacks of few layers.

ACKNOWLEDGMENTS

The financial support of the French National Research Agency (ANR) through the project TEAM2ClayDesicc (ANR-14-CE05-0023-01) is gratefully acknowledged.

REFERENCES

[1] K. Ioannidou, K.J. Krakowiak, M. Bauchy, C.G. Hoover, E. Masoero, S. Yip, F.-J. Ulm, P. Levitz, R.J.-M. Pellenq, E.D. Gado, Mesoscale texture of cement hydrates, Proc. Natl. Acad. Sci. (2016) 201520487. doi:10.1073/pnas.1520487113.

[2] T. Honorio, L. Brochard, M. Vandamme, Flexibility of clay layers and nanotexture, Submitt. Pap. (2017).

[3] S.A. Hamid, The crystal structure of the 11 Ä natural tobermorite Ca2.25[Si3O7.5(OH)1.5]·1H2O, Z. Für Krist. - Cryst. Mater. 154 (1981) 189–198. doi:10.1524/zkri.1981.154.14.189.

[4] I.G. Richardson, Tobermorite/jennite- and tobermorite/calcium hydroxide-based models for the structure of C-S-H: applicability to hardened pastes of tricalcium silicate, β-dicalcium silicate, Portland cement, and blends of Portland cement with blast-furnace slag, metakaolin, or silica fume, Cem. Concr. Res. 34 (2004) 1733–1777. doi:10.1016/j.cemconres.2004.05.034.

[5] K.J. Krakowiak, J.J. Thomas, S. Musso, S. James, A.-T. Akono, F.-J. Ulm, Nano-chemo-mechanical signature of conventional oil-well cement systems: Effects of elevated temperature and curing time, Cem. Concr. Res. 67 (2015) 103–121. doi:10.1016/j.cemconres.2014.08.008.

[6] R. Shahsavari, R.J.-M. Pellenq, F.-J. Ulm, Empirical force fields for complex hydrated calcio-silicate layered materials, Phys. Chem. Chem. Phys. 13 (2010) 1002–1011. doi:10.1039/C0CP00516A.

[7] M.J. Abdolhosseini Qomi, F.-J. Ulm, R.J.-M. Pellenq, Physical Origins of Thermal Properties of Cement Paste, Phys. Rev. Appl. 3 (2015) 064010. doi:10.1103/PhysRevApplied.3.064010.

[8] S. Masoumi, H. Valipour, M.J. Abdolhosseini Qomi, Intermolecular Forces between Nanolayers of Crystalline Calcium-Silicate-Hydrates in Aqueous Medium, J. Phys. Chem. C. 121 (2017) 5565–5572. doi:10.1021/acs.jpcc.6b10735.

[9] A.J. Allen, J.J. Thomas, H.M. Jennings, Composition and density of nanoscale calcium–silicate–hydrate in cement, Nat. Mater. 6 (2007) 311–316. doi:10.1038/nmat1871.

[10] S. Plimpton, Fast Parallel Algorithms for Short-Range Molecular Dynamics, J. Comput. Phys. 117 (1995) 1–19. doi:10.1006/jcph.1995.1039.

[11] O.L. Manevitch, G.C. Rutledge, Elastic Properties of a Single Lamella of Montmorillonite by Molecular Dynamics Simulation, J. Phys. Chem. B. 108 (2004) 1428–1435. doi:10.1021/jp0302818.

[12] L.D. Landau, E.M. Lifshitz, Theory of Elasticity, Pergamon Press, 1970. http://archive.org/details/TheoryOfElasticity (accessed March 16, 2017).

[13] M. Parrinello, A. Rahman, Strain fluctuations and elastic constants, J. Chem. Phys. 76 (1982) 2662–2666. doi:10.1063/1.443248.

[14] B. Militzer, H.-R. Wenk, S. Stackhouse, L. Stixrude, First-principles calculation of the elastic moduli of sheet silicates and their application to shale anisotropy, Am. Mineral. 96 (2015) 125–137. doi:10.2138/am.2011.3558.

[15] M. Youssef, R.J.-M. Pellenq, B. Yildiz, Glassy Nature of Water in an Ultraconfining Disordered Material: The Case of Calcium−Silicate−Hydrate, J. Am. Chem. Soc. 133 (2011) 2499–2510. doi:10.1021/ja107003a.

[16] U. Raviv, S. Perkin, P. Laurat, J. Klein, Fluidity of Water Confined Down to Subnanometer Films, Langmuir. 20 (2004) 5322–5332. doi:10.1021/la030419d.

[17] P.A. Bonnaud, C. Labbez, R. Miura, A. Suzuki, N. Miyamoto, N. Hatakeyama, A. Miyamoto, K.J.V. Vliet, Interaction grand potential between calcium–silicate–hydrate nanoparticles at the molecular level, Nanoscale. 8 (2016) 4160–4172. doi:10.1039/C5NR08142D.

[18] H. Manzano, E. Masoero, I. Lopez-Arbeloa, H.M. Jennings, Shear deformations in calcium silicate hydrates, Soft Matter. 9 (2013) 7333–7341. doi:10.1039/C3SM50442E.

[19] B. Carrier, Influence of water on the short-term and long-term mechanical properties of swelling clays : experiments on self-supporting films and molecular simulations, phdthesis, Université Paris-Est, 2013. https://pastel.archives-ouvertes.fr/pastel-00960833/document (accessed August 19, 2015).

[20] M. Zabat, R. Harba, H.V. Damme, Fractal analysis of surface roughness of montmorillonite clay self-supported films: Effects of exchanged cations and of mechanical tensile stress, Colloids Surf. Physicochem. Eng. Asp. 486 (2015) 38–44. doi:10.1016/j.colsurfa.2015.09.001.

[21] E. Masoero, E.D. Gado, R.J.-M. Pellenq, S. Yip, F.-J. Ulm, Nano-scale mechanics of colloidal C–S–H gels, Soft Matter. 10 (2013) 491–499. doi:10.1039/C3SM51815A.

[22] B. Jönsson, A. Nonat, C. Labbez, B. Cabane, H. Wennerström, Controlling the Cohesion of Cement Paste, Langmuir. 21 (2005) 9211–9221. doi:10.1021/la051048z.

[23] R.J.-M. Pellenq, N. Lequeux, H. van Damme, Engineering the bonding scheme in C–S–H: The iono-covalent framework, Cem. Concr. Res. 38 (2008) 159–174. doi:10.1016/j.cemconres.2007.09.026.